Experimental Investigation of the Influence of a Centered Line Sparger on the Jet from the Shroud in a 1:3 Water Model of a Tundish

Maria Thumfart, Arnis Pelss, and Herbert Pfeifer*

In a continuous casting plant a tundish serves two main purposes. Firstly, it is a buffer vessel between the ladles and the mold and secondly, it is designed to remove non-metallic particles from the melt. As the demands on the quality of the cast product have increased strongly, floatation (removal of particles using bubbles) of the particles becomes necessary. These bubbles alter the global flow field in the tundish. At large gas flow rates this influence needs to be considered in the positioning of mechanical flow control devices such as wears or impact pads. In this paper the influence of a line sparger on the global flow field is investigated using a 1:3 water model. A series of PIV (Particle Image Velocimetry) measurements have been performed at a wide range of air and water flow rates showing the influence of the bubbles on the shape of the liquid jet from the shroud. In addition, a dimensionless number is derived, which can be used to scale the gas flow rate from different experiments. This number is shown to be valid within the range of the experiments presented in this paper.

1. Introduction

In a continuous casting plant the liquid steel is transported in ladles to the caster. From the ladles the steel flows through the tundish to the mold. The tundish has two main purposes. Firstly, it is a buffer between the ladles and the mold, as the steel flow from the ladles is discontinuous. Secondly, it offers the possibility to separate non-metallic particles from the melt.[1] Accordingly, the tundish is a key instrument in clean steel production.

Non-metallic particles are buoyant in liquid steel. Hence, they tend to rise to the steel-slag interface, where they are trapped. This behavior can be supported by mechanical flow control devices like wears, dams or impact pads.[2–4] These devices can be used to increase the minimal and peak residence time of the steel in the tundish. Hence the particles have more time to rise.

This approach only works for large and medium sized particles, as the particle rise velocity decreases with its diameter. A theoretical optimum for the flow in the tundish was derived by Javurek.[5] He shows, that even at this optimum there is a lower border, for which particle size the tundish can reach sufficient separation rates. For smaller particles other separation mechanisms need to be considered.

One option to improve the separation rate is to introduce bubbles in the tundish. There are two different mechanisms reported in literature which improve the separation rate. At low gas flow rates, the bubbles positively influence the liquid flow field.[6,7] The influence of bubble particle collisions is neglected. At larger gas flow rates, the bubbles are used to collect particles and transport them to the surface.[4,8,9,10,14] This mechanism is called floatation and is already widely used in fields like paper recycling or ore production.[15]

Floatation works for all particles, which are badly wetting to their surrounding liquid, thus having a contact angle larger than 90°. Non-metallic inclusions like Al_2O_3 have a contact angle ranging from 80° to 138° depending on the steel grade.[16] Accordingly floatation is possible in steel production.

The optimal amount of gas bubbles inserted in the tundish is still under discussion. Reported gas flow rates range from well below $0.01\,l_{stp}\,min^{-1}$ up to $55\,l_{stp}\,min^{-1}$.[6–10] While the low gas flow rates can be expected to barely change the global flow field in the tundish, larger gas flow rates can induce large flow velocities, which can even deflect the jet coming from the ladle shroud. If this deflection becomes too large, the design of tundish insertions might be compromised.

The significance of the direction of the jet from the ladle shroud was shown by Chattopadhyay.[11,12] He inclined the shroud by about 4–5°. Even at this small inclination significant differences in the slag entrainment were measured.

The influence of argon injection in the tundish on the global velocity field is still often neglected. Cicutti[13] investigated the influence of an argon flow rate of $20\,l_{stp}\,min^{-1}$ on the inclusion removal rate of a two strand tundish in the course of plant trials. These experiments showed a better removal rate in the strand

M. Thumfart
K1-MET GmbH
Stahlstraße 14, 4020 Linz, Austria
E-mail: maria.thumfart@k1-met.com

Dr. A. Pelss, Prof. H. Pfeifer
RWTH Aachen
Institut für Industrieofenbau und Wärmetechnik
Kopernikusstr. 10, 52074 Aachen, Germany

DOI: 10.1002/srin.201800639

with the argon curtain compared to the strand without argon injection. The possible influence of the argon injection on the global velocity field in both strands is not mentioned.

The focus of the work presented in this paper is to quantify the influence of the bubbles on the jet deflection depending on the gas and liquid flow rate for a given geometry. In order to properly scale the gas flow rate, a force ratio is derived, which represents the experimental results well.

2. Experimental Setup

A water model (scale 1:3) of a 16 t single-strand tundish with a line sparger is used for the experiments. **Figure 1**a and **Table 1** summarize the dimensions of the experimental setup. The air flow rate is controlled by a mass flow controller (ANALYT-MTC 35837). The water flow rate is measured with a flow meter (Endress + Hauser Promag 53P65). The setup is filled with 20 °C tap water. The water temperature is checked before each experiment. A more detailed description of the used tundish can be found in Ref. [1,3].

Figure 1b shows the bubbles resulting from the line sparger at an air flow rate of $50\,l_{stp}\,min^{-1}$ and a water flow rate of $20\,l\,min^{-1}$. Photographs of the bubble curtain at additional water and air flow rate combinations can be found in the supporting material (Figure S1, S2, and S3, Supporting Information).

The water flow in the tundish is measured using a PIV-system (Particle Image Velocimetry). The particles (Vestosint 1111) added to the water have a density of $1016\,kg\,m^{-3}$ and an average diameter of 100 µm. They are introduced into the water mechanically without any additional chemicals. Two double frame cameras are used to take images of the particles in the right half and the left half of the tundish respectively. The PIV laser, a pulsed Nd:YAG laser, is placed in the center plane of the tundish as indicated in Figure 1a. The raw velocity fields are calculated using Davis. All additional calculations like the median filter and the time average calculation are implemented in Matlab.

3. Theoretical Considerations

In the field of metallurgical flows physical models are common practice. Especially water models are widely used. The key issue in physical modeling is the correct scaling of the experimental parameters. For the modeling of liquid steel flows without gas injection the Reynolds (*Re*) number and the Froude (*Fr*) number are relevant. In case of a 1:1 water model both similarities can be satisfied using a velocity ratio of one. In case of a 1:3 water model only one of the two similarities can be satisfied as shown by Equation (1) and (2).

$$Re = \frac{\rho L U}{\mu} \Rightarrow \frac{U_m}{U_p} = \frac{L_p}{L_m} = 3 \tag{1}$$

$$Fr = \frac{U}{\sqrt{Lg}} \Rightarrow \frac{U_m}{U_p} = \sqrt{\frac{L_m}{L_p}} = \sqrt{\frac{1}{3}} \tag{2}$$

For the experiments presented below the water flow rate ranges from Froude similarity to Reynolds similarity.

The focus of this paper is to investigate the influence of a bubble curtain on the shape of the jet from the shroud. Accordingly the gas flow rate needs to be scaled as well. Scaling laws for bubbly flows often include the Weber number or a modified Froude number. The Weber similarity leads to similar bubble sizes if geometric similarity and similar wetting conditions can be ensured. The modified Froude number is a ratio between the gas momentum at the injection nozzle and the buoyancy force. Hence it describes the penetration depth of a horizontal bubble jet.[17]

The purpose of the measurements presented in this paper is to show the influence of the bubbles on the global flow field. The most significant impact is a deflection of the center line of the liquid jet from the shroud. None of the scaling laws mentioned above includes a force ratio appropriate to scale this effect. Accordingly it is necessary to take a closer look at the main forces in the tundish.

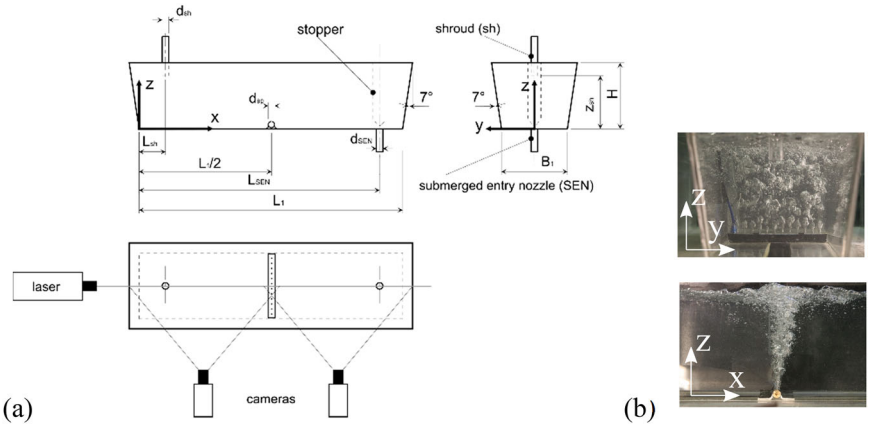

Figure 1. a) Dimensions of the experimental setup and PIV placement. b) Line sparger at an air flow rate of $50\,l_{stp}\,min^{-1}$ and a water flow rate of $20\,l\,min^{-1}$.

Table 1. Dimensions of the experimental setup.

Description	Symbol	Unit	Plant	Model
Volume of tundish at filling level H	V	m^3	2.275	0.084
Tundish length	L_1	m	3.140	1.047
Tundish width	B_1	m	0.780	0.26
Inclination of the side walls	γ	°	7	7
Filling level	H	m	0.8	0.266
Shroud-bottom distance	z_{sh}	m	0.6	0.2
Shroud position	L_{sh}	m	0.335	0.122
Shroud diameter	d_{sh}	m	0.068	0.023
SEN position	L_{SEN}	m	2.885	0.962
SEN diameter	d_{SEN}	m	0.070	0.023
Sparger outer diameter	d_{sp}	m		0.02
Sparger pore diameter	d_p	m		0.002
Number of pores	n_p			12

The integral form of the momentum balance in the tundish calculates to

$$\oint p\vec{n}\mathrm{d}A + \oint \vec{v}\vec{v}\vec{n}\mathrm{d}A = \int \rho\vec{g}\mathrm{d}V \tag{3}$$

Taking the tundish content as a control volume only two major forces are left. The first is the buoyancy of all the bubbles present in the tundish

$$F_B = \int \left(\rho_l - \rho_g\right)\mathrm{g}\mathrm{d}V_g = V_g(\rho_l - \rho_g)g \tag{4}$$

This equation contains the integral volume of all gas bubbles in the tundish V_g. This volume can be estimated using the gas volume flow rate Q_g, the tundish fill level h_t and the average bubble rise velocity v_r.

$$V_g = \frac{Q_g h_t}{v_r} \tag{5}$$

The second is the jet momentum. It can be calculated from the liquid velocity at the end of the shroud.

$$F_J = \rho_l \int v_s^2 \mathrm{d}A_s = \rho_l Q_l^2 \frac{c}{A_s} \tag{6}$$

with the shroude cross section A_s. Accordingly the ratio of the two forces (Equation (4) and (6)) calculates to

$$\frac{F_B}{F_J} = \underbrace{\frac{Q_g}{Q_l^2}}_{\text{flow ratio}} \quad \underbrace{\frac{1}{v_r}}_{\text{system parameter}} \quad \underbrace{\frac{A_s g h_t}{c}}_{\text{constants}} \quad \underbrace{\frac{\rho_l - \rho_g}{\rho_l}}_{\sim 1} \tag{7}$$

As the density of the gas phase is much smaller than the density of the liquid phase, the ratio of the density difference and the liquid density can be neglected. The remaining variables can be categorized into three different groups:

- Constants: these values are the same for all experiments presented in this paper
- System parameter: The average rise velocity of the gas phase v_r depends on the overall flow situation in the tundish, the bubble size distribution, the bubble density in the tundish and the bubble Reynolds number. For the experiments presented in this paper it is assumed to be approximately constant. This assumption is not valid if Equation (7) is used to transfer results from a water model to the plant. In this case the difference between the bubble rise velocity in the water model and the plant needs to be calculated.
- Flow ratio: The gas and liquid flow rates have been changed within a large range of values.

Accordingly the flow ratio

$$f_Q = \frac{Q_g}{Q_l^2} \tag{8}$$

will be used to represent the experimental results.

Table 2. Number of measurements at the different settings.

		Setpoint normalized volume flow rate of air $[l_{stp}\,min^{-1}]$				
Number of measurements		0	25	50	75	100
Setpoint volume flow rate water in $[l\,min^{-1}]$	20	3	4	4	4	4
	30	3	4	4	4	4
	40	3		2		2
	50	3		2		2
	60	3				2
	80	3				2
	96	2				2

4. Experimental Results

As already mentioned in chapter 2, in the case of a 1:3 water model the water flow rate can either be chosen to fit the Froude similarity or the Reynolds similarity. The reference case for the measurements here is a steel flow rate of $320\,l\,min^{-1}$ which represents a mass flow rate of steel of approximately $2.3\,t\,min^{-1}$. Considering the Froude number as scaling law this results in a water flow rate of $20\,l\,min^{-1}$. Considering the Reynolds number it results in a water flow rate of $96\,l\,min^{-1}$. In order to receive a sound benchmark database, the water flow rate range was chosen from $20\,l\,min^{-1}$ to $96\,l\,min^{-1}$. This results in a larger set of data points to evaluate the dimensionless number.

The argon flow rates in the tundish reported in literature range from well below $0.01\,l_{stp}\,min^{-1}$ to $55\,l_{stp}\,min^{-1}$[6–10] measured at standard conditions and referring mostly to the industrial case. These standard conditions usually are 20 °C and 1 bar. Accordingly, this gas flow rate needs to be multiplied by the

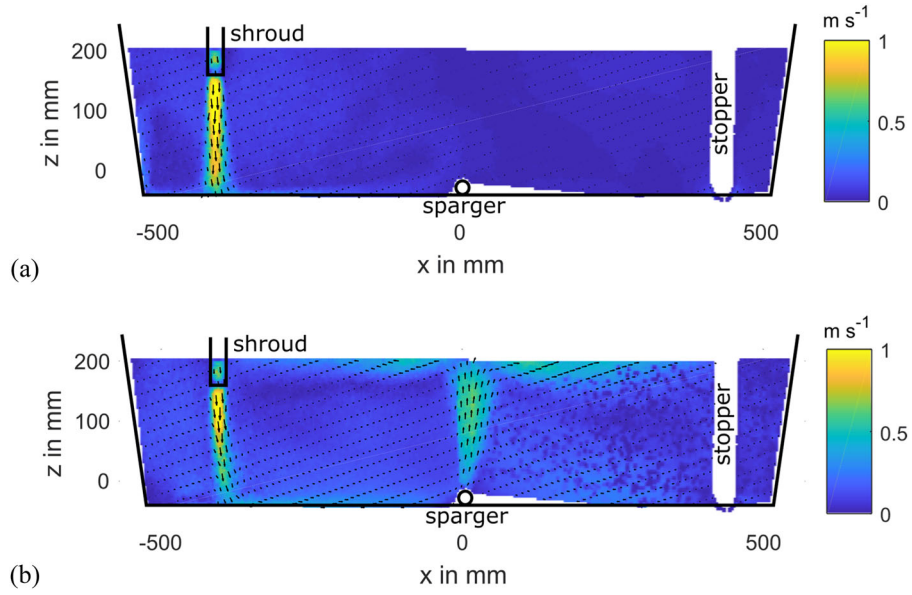

Figure 2. Averaged velocity magnitude in m s^{-1} at a water flow rate of 30 m min^{-1} and an air flow rate of (a) 0 l_{stp} min^{-1} and (b) 100 l_{stp} min^{-1}. The badly illuminated areas near the sparger and the free surface have been masked. The mask at the surface starts 30 mm bellow the fill level to prevent errors from light reflections at the surface.

temperature ratio resulting in an actual volume flow rate in the tundish of up to 330 l min^{-1}.

In the experiments presented in this paper the focus is on the influence of the bubbles on the deflection of the jet from the shroud. Accordingly, the upper range of gas volume flow rate has been chosen as a reference. In order to scale the gas flow rate from the tundish to the water model Equation (7) is used.

$$\frac{Q_{g,p}}{Q_{l,p}^2}\frac{1}{\nu_{r,p}}\frac{A_{s,p}gh_{t,p}}{c} = \frac{Q_{g,m}}{Q_{l,m}^2}\frac{1}{\nu_{r,m}}\frac{A_{s,m}gh_{t,m}}{c} \tag{9}$$

The volume flow rate scales accordingly with

$$\frac{Q_{g,m}}{Q_{g,p}} = \frac{L_m}{L_p}\left(\frac{U_{l,m}}{U_{l,p}}\right)^2\frac{\nu_{r,m}}{\nu_{r,p}} \tag{10}$$

The velocity ratio in Equation (10) is the ratio between water velocity in the model $U_{l,m}$ and steel velocity in the plant $U_{l,p}$. The rise velocity of the argon bubbles in the tundish is not reported by Kumar.[8] But even assuming the bubble rise velocity is equal in the model and the real tundish, the gas flow rate ranges between 37 l min^{-1} (using the liquid velocity ratio from Froude

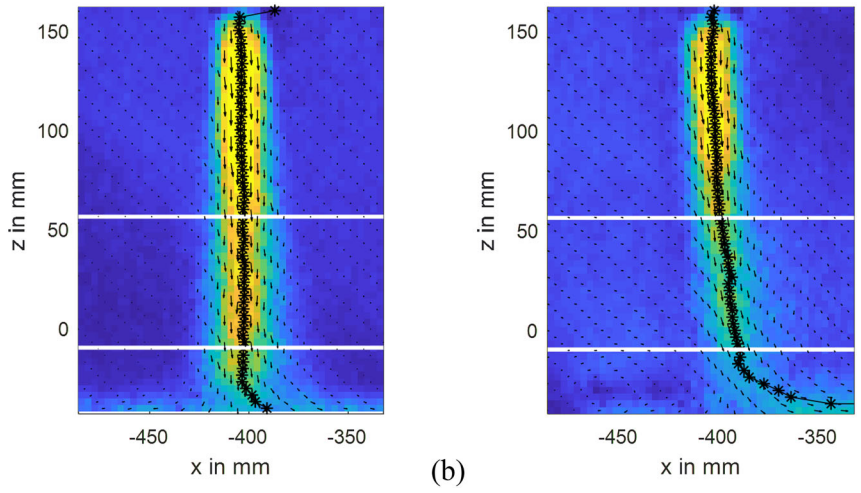

Figure 3. Detected jet center (black stars) at a water volume flow rate of 30 m min^{-1} and an air flow rate of (a) 0 l_{stp} min^{-1} (almost no deflection) and (b) 100 l_{stp} min^{-1} (positive deflection). The white horizontal lines indicate the region of interest.

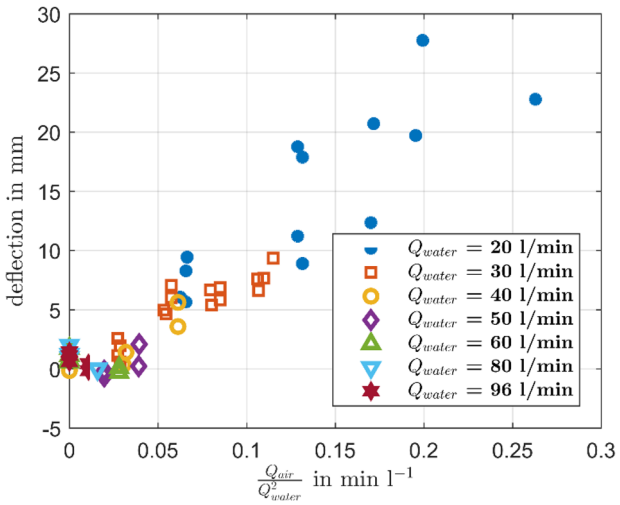

Figure 4. Average deflection of the jet from the shroud within the region of interest indicated in Figure 3.

similarity) and 990 l min^{-1} (using the liquid velocity ratio from Reynolds similarity). These calculations only indicate the order of magnitude for the air flow rate in the experiment. In accordance with the limitations of the experimental setup the air flow rates range from 0 l_{stp} min^{-1} to 100 l_{stp} min^{-1}.

Table 2 shows the number of measurements taken at each set of volume flow rates. A measurement is a set of 70 snapshots of the velocity field gained from the PIV measurements at a frequency of 7 Hz. For some settings the measurements have been repeated at several measurement days in order to evaluate the reproducibility of the results. The velocity fields were filtered (median filter) and averaged with respect to time. **Figure 2** shows the resulting velocity magnitude for two examples. Figure 2a shows the average velocity field at a water flow rate of 30 l min^{-1} without air. The sparger in the middle of the tundish induces a weak recirculation area. Figure 2b shows the same water flow rate as Figure 2a but with an air flow rate of 100 l_{stp} min^{-1}. The rise in flow velocity can be observed in almost all parts of the tundish. The velocities in the bubble plume and at the right side of it are prone to error as the laser sheet is scattered by the bubbles.

In order to detect the jet deflection in the *x*-*z*-plane it is necessary to detect the center of the jet. For the present measurements the data has been evaluated line by line. For each line a Gaussian curve has been fitted to the velocity magnitude. The position of the maximum of the Gaussian curve has been used as jet center. The result can be seen in **Figure 3**. The average *x*-position of the jet center in the region of interest $z \in [-10, 56]$ mm was defined as the jet deflection. This approach is necessary as the point of impact at the tundish bottom is hard to define from the measurements as can be seen in Figure 3b.

Figure 4 shows all the detected deflection values in one graph. The differnt symbols represent different water flow rates. With rising air flow rates up to an f_Q of 0.03 min l^{-1} the deflection stays almost zero. Only for larger air flow rates a deflection of the jet was detected.

Figure 4 shows that, using the volume flow ratio f_Q all the deflection curves match well. For instance at $f_Q = 0.06$ min l^{-1} the deflection values of three different water flow rates meet. Accordingly Equation (7) is valid within the set of parameters presented in this paper.

5. Conclusion

The main goal of the experiments presented in this paper was to quantify the influence of bubbles on the global flow field of a tundish. It could be shown that the flow induced by the used line sparger was strong enough to deflect the jet from the shroud significantly. Accordingly this effect needs to be considered in the design of mechanical flow control devices.

In addition the main forces influencing the flow field were identified and related to the flow parameters. This resulted in a force ratio which can be used to scale critical gas flow rates depending on the liquid flow rate and the system parameters to limit the deflection of the jet.

6. Outlook

The results of this experimental investigation are used to evaluate the accuracy of different simulation approaches for a tundish with a sparger. The results of these simulations are published by Holzinger.[18]

Supporting Information

Supporting Information is available from the Wiley Online Library or from the author.

Acknowledgements

The authors gratefully acknowledge the funding support of K1-MET GmbH, metallurgical competence center. The research program of the competence center K1-MET is supported by COMET (Competence Center for Excellent Technologies), the Austrian program for competence centers. COMET is funded by the Federal Ministry for Transport, Innovation and Technology, the Federal Ministry for Science, Research and Economy, the province of Upper Austria, Tyrol, and Styria, the Styrian Business Promotion Agency.

Conflict of Interest

The authors declare no conflict of interest.

Nomenclature

A surface area in m^2
c constant describing shroud velocity profile
Fr Froude number
f_Q volume flow ratio in min l^{-1}
g gravitational acceleration in m s^{-2} or subscript for gas
h_t Tundish fill level in m
L typical length of the model or the plant in m
l subscript for liquid
m subscript for model
$\vec{n}$ normal vector to surface
p pressure in Pa or subscript for plant

Q volume flow rate in $m^3 s^{-1}$
Re Reynolds number
s subscript for shroud
U typical velocity of the model or the plant in $m s^{-1}$
$\vec{v}$,v velocity in $m s^{-1}$
v_r bubble rise velocity in $m s^{-1}$
V volume in m^3
μ dynamic viscosity in Pa s
ρ density in $kg m^{-3}$

Keywords

bubble curtain, dimensionless constants, jet deflection, line sparger, PIV measurements scale up, tundish

Received: December 20, 2018
Revised: March 14, 2019
Published online: April 8, 2019

[1] A. Rückert, M. Warzecha, R. Koitzsch, M. Pawlik, H. Pfeifer, *Steel Res. Int.* **2009**, *80*, 8.
[2] G. Solorio-Diaz, J. A. Ramos-Banderas, J. de Barreto, R. D. Morales, *Steel Res. Int.* **2008**, *80*, 3.
[3] H. Odenthal, R. Bölling, H. Pfeifer, *Steel Res. Int.* **2003**, *74*, 1.
[4] Z. Meijie, G. Huazhi, H. Ao, Z. Hongxi, D. Chengji, *J. Min. Metall.* **2011**, *47*, 2.
[5] M. Javurek, *PhD Thesis*, Johannes Kepler University (Linz, Austria), January, **2006**.
[6] A. Ramos-Banderas, R. D. Morales, J. de Barreto, G. Solorio-Diaz, *Steel Res. Int.* **2006**, *77*, 5.
[7] L. Zhong, L. Li, B. Wang, M. Jiang, L. Zhu, L. Zhang, R. Chen, *Steel Res. Int.* **2006**, *77*, 2.
[8] D. S. Kumar, T. Rajendra, R. Prasad, A. Sarkar, M. Ranjan, *Ironmaking Steelmaking* **2009**, *36*, 6.
[9] A. Cwudziński, *Steel Res. Int.* **2009**, *81*, 2.
[10] A. Cwudziński, *Steel Res. Int.* **2017**, *88*, 9.
[11] K. Chattopadhyay, F. G. Liu, M. Isac, R. I. L. Guthrie, *Ironmaking Steelmaking.* **2010**, *38*, 2.
[12] K. Chattopadhyay, F. G. Liu, M. Isac, R. I. L. Guthrie, *ISIJ Int.* **2011**, *51*, 5.
[13] C. Cicutti, A. Martin, J. Mendez, M. Romero, G. di Gresia, *Proceedings of the 7th European Continuous Casting Conf.* **2011**.
[14] L. Zhang, J. Aoki, B. G. Thomas, *Metall. Mater. Trans B* **2006**, *37B*, 361.
[15] G. Holzinger, *PhD Thesis*, Johannes Kepler University (Linz, Austria), September **2016**.
[16] A. Karasangabo, *PhD Thesis*, University of Leoben (Austria), January **2009**.
[17] C. Wuppermann, N. Giesselmann, A. Rückert, H. Pfeifer, H. Odenthal, E. Hovestädt, *Steel Res. Int.* **2012**, *52*, 10.
[18] G. Holzinger, M. Thumfart, *Steel Res. Int.* srin201800642 submitted **2018**.